FISEVIER

Contents lists available at ScienceDirect

Palaeogeography, Palaeoclimatology, Palaeoecology

journal homepage: www.elsevier.com/locate/palaeo



Organic matter sources and lateral sedimentation in a Bahamian karst basin (sinkhole) over the late Holocene: Influence of local vegetation and climate



Anne E. Tamalavage^{a,*}, Peter J. van Hengstum^{a,b}, Patrick Louchouarn^{a,b}, Sergey Molodtsov^a, Karl Kaiser^{a,b}, Jeffrey P. Donnelly^c, Nancy A. Albury^d, Patricia L. Fall^e

- ^a Department of Oceanography, Texas A&M University, College Station, TX 77843, USA
- ^b Department of Marine Sciences, Texas A&M University at Galveston, Galveston, TX 77554, USA
- ^c Coastal Systems Group, Woods Hole Oceanographic Institution, Woods Hole, MA 02543, USA
- ^d National Museum of The Bahamas, PO Box EE-15082, Nassau, the Bahamas
- e Department of Geography and Earth Sciences, University of North Carolina Charlotte, Charlotte, NC 28223, USA

ARTICLE INFO

Keywords: Stable isotopes Mixing model Karst Subtropical landscape Caribbean

ABSTRACT

Karst basins (e.g., blueholes, sinkholes) accumulate well-preserved sedimentary successions that provide transformative paleoclimatic and paleoenvironmental information. However, the sedimentary processes within these basins are not yet fully understood. Here we present stable carbon isotopic values ($\delta^{13}C_{org}$) and C:N ratios of bulk organic matter in well-dated sediment cores from Blackwood Sinkhole (Abaco, The Bahamas) to investigate the changing flux of organic matter into the sinkhole during the late Holocene. The provenance of preserved organic matter changed through the late Holocene between three primary sources, as determined by three-endmember mixing modeling: wetland organic matter from the adjacent epikarst surface, authigenic primary productivity in the oligohaline meteoric lens, and terrestrial organic matter from the surrounding landscape. Expansion of wetlands on the adjacent epikarst surface played a critical role by increasing the flux of wetland organic matter to the sinkhole, especially during the last 1000 years. Hurricanes and regional rainfall may have mediated organic matter delivery to the benthos, either through hampering wetland development (prior to 1000 cal yr BP) or by changing dissolved nutrient concentrations available in the basin for primary producers. These results demonstrate that organic matter provenance in karst basins is not constant through time, and is significantly dependent upon both landscape vegetation on the epikarst surface and changing hydrographic conditions that impacts nutrient availability to primary producers.

1. Introduction

The sediment in karst basins (e.g., sinkholes, blueholes) provides useful paleoclimate and paleoecological information from carbonate landscapes. In general, the Holocene parasequence on North Atlantic carbonate platforms is relatively thin, with preservation potential limited by local sediment re-working (physical and biological) or off-bank sediment export (Rasmussen et al., 1990; Mackinnon and Jones, 2001; Maloof and Grotzinger, 2012). In contrast, karst basins are natural sediment and fossil traps that develop from subsurface dissolution and collapse of antecedent carbonates during the Quaternary (Mylroie et al., 1995; Shinn et al., 1996; Smart et al., 2006). Their often dysoxic to anoxic bottom water leads to excellent sediment preservation that is useful for developing records of hydroclimate and environmental change.

For example, fossil pollen composition in Floridian and Bahamian

karst basins documents centennial to millennial-scale climate change (Grimm et al., 1993; Kjellmark, 1996). Microfossil ecology (e.g., foraminifera, ostracodes) has been used to document long-term groundwater salinity changes (Teeter, 1989; Alverez Zarikian et al., 2005; van Hengstum et al., 2010), and microfossil geochemistry can document local evaporation-precipitation ratio changes (Hodell et al., 2001; Hodell et al., 2005). Deposits in karst basins have transformed knowledge of regional faunal changes (Hearty et al., 2004; Steadman et al., 2014), while more recently, coarse-grained overwash deposits in coastal systems have been used to generate paleo hurricane reconstructions (Lane et al., 2011; Denomee et al., 2014; van Hengstum et al., 2014). However, investigation of the sedimentary processes that operate within karst basins remains an area of active research, which is required for accurate interpretation of paleo records from karst basins.

Arguably, the most important variable influencing lifetime sedimentary processes within sinkholes during the Quaternary is the

E-mail address: atamalavage91@tamu.edu (A.E. Tamalavage).

^{*} Corresponding author.

relationship between the elevation of the karst basin in the carbonate and local groundwater level, which is largely driven by eustatic sealevel change (Richards et al., 1994; Dutton et al., 2009; van Hengstum et al., 2011). The direct infiltration of meteoric water into subsurface aquifers means that fluvial-style sedimentary processes and landforms are limited on the subaerial surface of carbonate landscapes. Similar to large, dish-shaped depressions on the antecedent carbonate surface (Ashmore and Leatherman, 1984; Rasmussen et al., 1990; Mackinnon and Jones, 2001), karst basins are inundated first from within by concomitant groundwater and sea-level rise. Eventually, offshore blueholes are created if continual sea-level rise completely inundates a karst basin (Shinn et al., 1996). This creates a natural lifetime progression of sedimentary processes influenced first by terrestrial conditions, then mixed aquatic and terrestrial conditions, and finally marine conditions during a transgressive event (Shinn et al., 1996; Gregory et al., 2015).

Recent work indicates sedimentation in partially flooded karst basins is complex, and influenced by multiple factors. For example, sedimentation is impacted by erosion of terrestrial soils and aquatic organic matter (van Hengstum et al., 2010), fluctuations in primary productivity (van Hengstum et al., 2018), variable inorganic mineral production (Kovacs et al., 2017), the transport and delivery of sediment through biologic vectors (Collins et al., 2015a), and the morphology of conduits and the basin itself (Gregory et al., 2016). Vegetation on the land surface is also significant, because wetlands can either increase (by increasing sediment supply, Collins et al., 2015b) or decrease (by baffling sediment flux, Gregory et al., 2016) sedimentation in adjacent karst basins. Regardless, bulk organic matter is a dominant component of sediment records from karst basins, and the ability to deconstruct the provenance and quantity of organic matter through time would better inform regional paleoenvironmental change.

This study investigates organic matter provenance in a terrestrial sinkhole during the late Holocene where: (a) significant shifts in terrestrial and aquatic flora have been reported from co-stratigraphic pollen records, (b) the adjacent coastline experienced multi-decadal changes in intense hurricane activity, and (c) the adjacent epikarst surface experienced wetland expansion during the late Holocene. More specifically, we analyze the stable carbon isotopic ratio $(\delta^{13}C_{\rm org})$ and C:N ratio of bulk organic matter in well dated late Holocene sediment successions, and apply a three end-member mixing model to investigate how and why (based on local vs. climate drivers) organic matter provenance in the sediment record has changed through time.

2. Study site

The Bahamas are a group of carbonate islands and banks covering 300,000 km² in the North Atlantic Ocean (Carew and Mylroie, 1997), in which emergent islands make up 5.5% of the total area (Mylroie et al., 1995; Whitaker and Smart, 1997). Geologically, the islands are typically low-lying and preferentially occur on the eastern side of the banks due to build up associated with northeastly trade winds. These conditions result in topographically elevated eolianite ridges limited to the windward side of the island (Carew and Mylroie, 1997; Whitaker and Smart, 1997). The northernmost Bahamian carbonate platform is Little Bahama Bank (26.79°N, 77.42°W), characterized by two large islands: Grand Bahamas and Great Abaco Island (Walker et al., 2008). Blackwood Sinkhole is located 220 m from the northeastern shoreline on Great Abaco Island (Fig. 1). The sediment within the sinkhole is lacking marine bioclasts and reef-dwelling foraminifera that are abundant in the adjacent modern beach sediment. It is likely that the sediment accumulating within the sinkhole is dominated by the adjacent terrestrial and mangrove environments that are less than ~220 m away (van Hengstum et al., 2016).

Tidal range in Abaco is ~ 1 m, and given the proximity of Blackwood Sinkhole to the ocean, the water level in the sinkhole is effectively sea level. Blackwood Sinkhole has a surface expression as a ~ 32 m diameter sinkhole lake, with a depth to the sediment-water interface in the

primary basin ranging from 33 to 38 m below sea level (mbsl). A secondary, cylindrical karst feature (ranging from ~46 to 61 mbsl, and known as 'The Pit') is connected to Blackwood Sinkhole through a cave tunnel at 32 mbsl that ranges in depth from ~46 to 61 mbsl (Fig. 2). This secondary basin has not yet experienced ceiling collapse. The sinkhole is bordered by significant wetland development on the eastern periphery (Fig. 1C), and is a groundwater-fed basin that receives no stream discharge. The sinkhole is hydrographically stratified, with surface salinity in the low oligohaline range (1.8 psu on date of analysis) and anoxic, saline groundwater from 15 to 40 mbsl (Fig. 1D).

Rainfall in the tropical North Atlantic is characteristically bimodal. with a dry season from November through April, and a wet season from May to October that is interrupted by a 'Mid-Summer Drought' (Magaña et al., 1999; Jury et al., 2007; Gamble et al., 2008). In Abaco, the rainy season occurs from June to December with the Mid-Summer Drought occurring in July to August (Jury et al., 2007). The dry season extends from December to June (Jury et al., 2007). The mean annual precipitation on Abaco Island is approximately 1400 mm yr⁻¹ from data accumulated for a 31-year time period (1951-1981). Modern vegetation on Abaco Island consists of an upper canopy of Bahamian pine and an understory of tropical hardwoods. However, low topographic areas support a 'coppice vegetation' that includes poisonwood (Metopium toxiferum), cassada wood (Bumelia salicifolia), tetrazigia (Tetrazigia bicolor), five-finger/chicken toe (Tabebuia bahamensis), quicksilver (Thouinia discolor), saw palmetto (Serenoa repens), among others (Kjellmark, 1996; Steadman et al., 2007; Slayton, 2010).

3. Methods

Sediment cores were collected from Blackwood Sinkhole (BLWD-C2: 2011, BLWD-C3: 2015; Fig. 2) using advanced technical scuba diving procedures following guidelines established by the American Academy of Underwater Sciences. An earlier sediment core is not analyzed here (BLWD-C1) due to stratigraphic evidence for slumping (van Hengstum et al., 2016). A push core was also collected from an area with the most expanded peat succession in the adjacent wetland (2015: BLWD-C6), which was located by mapping undulations in the underlying eolianite with a sediment probe (Fig. 1C). After collection, sediment cores were split lengthwise in the laboratory, visually described following Schnurrenberger et al. (2003), photographed, X-radiographed, and subsequently stored at 4°C prior to analysis. Variability in coarse fraction was analyzed using the Sieve-first Loss-on-Ignition (Sieve-first LOI) procedure (van Hengstum et al., 2016). This procedure is well suited for measuring coarse sediment fraction variability in highly heterogeneous sediments from lakes on carbonate landscapes. Contiguous 0.5-cm (BLWD-C2) or 1-cm (BLWD-C3, C6) sediment subsamples (volume 2.5 cm³) were wet sieved using 63-µm mesh, ovendried for 12 h at 60 °C, and weighed to determine the original sediment mass. Afterwards, samples were ignited for 4.5 h at 550 °C in a muffle furnace to remove OM and to concentrate the remaining mineral residue (Dean Jr, 1974; Heiri et al., 2001). The proportion of coarse sediment was then expressed as mass per unit volume ($D_{>63um}$ mg cm⁻³). Previously generated pollen data from BLWD-C2 were used for comparison to the present study (Fall et al., unpublished results; van Hengstum et al., 2016).

To establish age control for the cores, terrestrial plant macrofossils (e.g., twigs, leaves) were radiocarbon dated at National Ocean Sciences Accelerator Mass Spectrometry at Woods Hole Oceanographic Institution (Table 1). Conventional radiocarbon age results were calibrated into calendar years before present (cal yr BP) with IntCAL13, using 1950 CE as present (Reimer et al., 2013). Final downcore Bayesian age models for BLWD-C2 and BLWD-C3 were computed using the R program *Bacon v2.2* (Fig. 3), which provides probability estimates at each core depth (Blaauw and Christen, 2011).

Geochemical proxies such as $\delta^{13}C_{org}$ and $\delta^{15}N_{org}$, total organic carbon (TOC), total nitrogen (TN), and atomic C:N ratios are useful

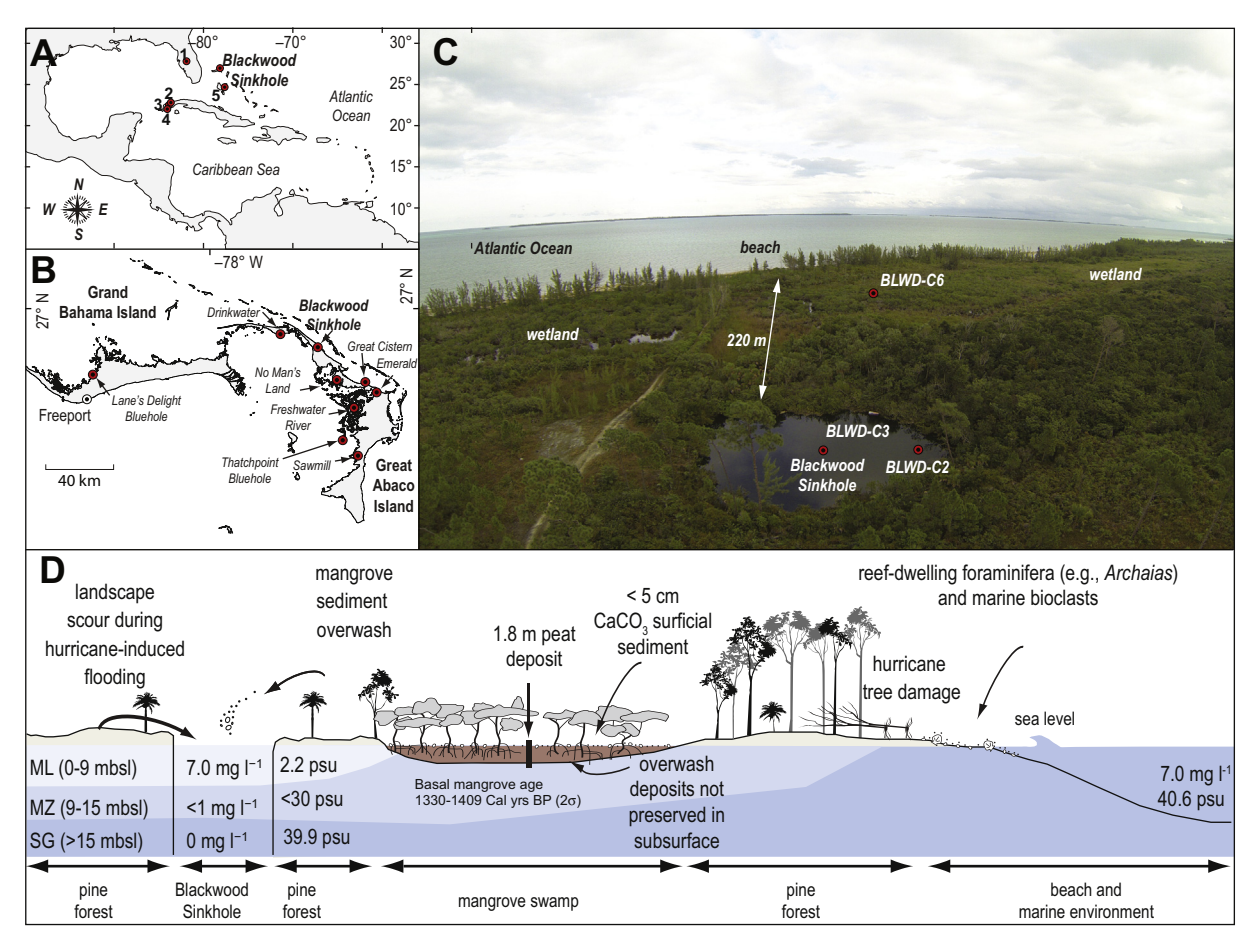


Fig. 1. (A) Map of the study area. Blackwood Sinkhole in in the western North Atlantic region. Other locations discussed in this study (1) Lake Tulane, Florida (Grimm et al., 2006); (2) Dos Anas cave system, Cuba (Fensterer et al., 2012); (3) Dos Anas and Santo Tomas cave system, Cuba (Fensterer et al., 2013); (4) Playa Bailen and Punta de Cartas, Cuba (Gregory et al., 2015); and (5) Church's Bluehole, offshore Andros Island, Bahamas (Kjellmark, 1996). (B) Islands on the Little Bahama Bank (Grand Bahama Island and Great Abaco Island) noting the locations of sinkholes and blueholes mentioned in the text. (C) Aerial photograph of Blackwood Sinkhole facing a northeasterly direction. Note that the row of trees along the beach edge is the invasive *Casurina* (Australian pine). (D) Conceptual model of the landscape surrounding Blackwood Sinkhole and some modern sedimentary processes (modified after van Hengstum et al., 2016). The minimum age for emplacement of the wetland on the epikarst surface is 1330–1409 (2σ calibrated result). Primary features (meteoric lens, mixing zone, saline groundwater) in the local coastal aquifer are defined by groundwater hydrographic variability (as mbsl, or meters below sea level), dissolved in O_2 (in mg L^{-1}), and salinity in psu. Acronyms: Meteoric Lens (ML), mixing zone (MZ), saline groundwater (SG).

tracers of organic matter provenance within coastal environments (Peters et al., 1978; Hedges et al. 1997; Lamb et al., 2006). Each core was sampled contiguously sampled for geochemical analysis. For BLWD-C2, a 5 mm sub-sample was obtained every 1 cm downcore from 0 to 110 cm, and isotopic analysis was conducted on samples taken every 1 cm (n = 110). A 1-cm interval was sampled from BLWD-C3 (n = 127), and a 1 cm sub-sample was obtained from BLWD-C6 everyother 2 cm (disregarding the upper 6 cm due to large root fragments) (n = 49). First, Total Carbon (TC) and Total Nitrogen (TN) were measured on freeze-dried 5 mg bulk sediment samples (not acidified) using a Costech™ 200 Elemental Analyzer, the TN was subsequently used in the C:N ratio calculation. Data calibration was determined relative to acetanilide and standard reference material for marine sediments according to the National Institute of Standards and Technology (NIST). A separate 100 mg sediment sample was then subjected to wet acidification with 8 mL of 1 M hydrochloric acid for 24 h, or until effervescence ceased, then desiccated at 50°C, and re-homogenized. The $\delta^{13}C_{org}$ and δ¹⁵N_{org} ratios of bulk organic matter, in addition to TOC and TN of the acidified sediment sub-samples, were measured at the Baylor University Stable Isotope Laboratory by a Thermo-Electron Delta V Advantage Isotope Ratio Mass Spectrometer. Final isotopic ratios are reported relative to the standard Vienna Pee Dee Belemnite (VPDB) for carbon and atmospheric nitrogen (expressed as parts per mil [%]). Analytical

precision for two international standards, USGS 40 and 41 which represent a range of $\delta^{13} C$ and $\delta^{15} N$ values for a two-point calibration, are within 0.2% (1 σ) for $\delta^{15} N$ and < 0.1% (1 σ) for $\delta^{13} C$. An additional internal standard (acetanilide) was used as an internal check for reproducibility, sample replicates are within a yielded a mean precision of 5.0%. The potential loss of carbon from the direct acidification process was corrected by multiplying the percent of sample remaining (post-acidification weight subtracted from pre-acidification weight/pre-acidification weight) and the TC% value measured after direct acidification (taken with isotopic measurements) for TOC (%) values. TOC% was divided by TN% (unacidified) and multiplied by the molecular weight ratio (14.01/12.01) to calculate the atomic C:N ratio.

4. Endmember analysis and mixing model implementation

Samples of modern particulate organic matter were obtained from several other karst basins on Abaco and the coastal ocean to examine as possible endmembers (Table 2). Modern water samples (1.5 L) were collected at 1 m water depth in the center of the sinkhole, and vacuum pumped through a combusted 47 μm GF/F filter. Filters were fume acidified with concentrated HCl for 24 h. Modern particulate organic matter samples were run for $\delta^{13}C_{org},\ \delta^{15}N_{org},\ and\ C:N$ analyses at the Texas A&M University Stable Isotope Geoscience Facility, processed on

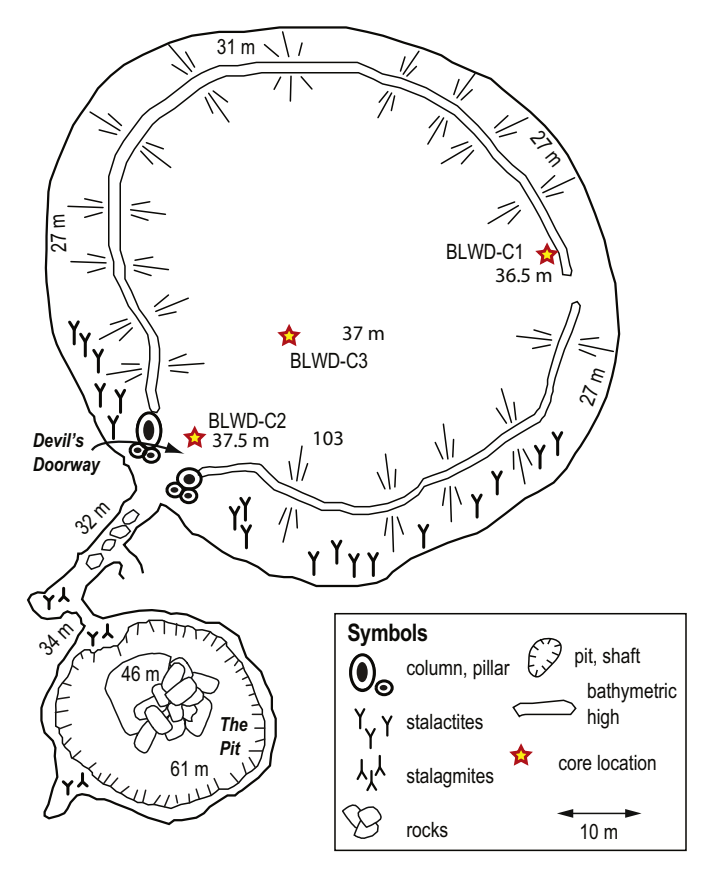


Fig. 2. Position of the sediment cores in Blackwood Sinkhole.

an Erba NA 1500 Elemental Analyzer, coupled with a Thermo Scientific DELTA plus isotope ratio mass spectrometer. Final isotopic ratios are reported relative to the standard Vienna Pee Dee Belemnite (VPDB) for Carbon and atmospheric Nitrogen for Nitrogen in per mil (‰). Analytical precision for two international standards, USGS 40 and 41a which represent a range of $\delta^{13}C$ and $\delta^{15}N$ values for a two-point calibration, are within 0.2‰ (1 σ) for $\delta^{15}N$ and $\delta^{13}C$. Additional internal standards (rice and acetanilide) were used as an internal check for reproducibility.

Indeed, it cannot be assumed that seston is debris only from living organisms, as the geochemical signature of seston can be biased by non-living organic matter particles (Yang et al., 2014). However, the average $\delta^{13}C_{org}$ value of the collected particulate organic matter from blueholes and sinkholes in Abaco is -35%, while the particulate organic matter from the ocean located 200 m east from Blackwood Sinkhole was -25%. This result is markedly consistent with a compilation of the $\delta^{13}C_{org}$ value of freshwater phytoplankton of $-32\pm3\%$ (France, 1995). As such, the particulate organic matter collected from the local karst basins is likely derived from primary producers in the sinkhole basin.

The sediment core collected from the adjacent wetland (BLWD-C6) was analyzed as a potential sediment source of wetland organic matter. In BLWD-C6, the long-term geochemical signal likely reflects both increased deposition of organic matter through time and geochemical degradation (diagenesis) from microbial activity. The $\delta^{13}C_{org}$ value of the bulk organic matter ranges from -28 to -26%, with a mean $\delta^{13}C_{org}$ of -26.6% \pm -0.5 (Fig. 4). The mean $\delta^{15}N_{org}$ is 3.3% \pm 1.6%. However, there is a significant downcore trend in both $\delta^{15}N_{org}$ values and C:N from 1 to 6% and $\sim\!14$ to 33, respectively. This enrichment in $\delta^{15}N_{org}$ values may be related to the preferential preservation of OM with a heavier $\delta^{15}N_{org}$ (Gonneea et al., 2004), or enhanced diagenesis of the organic matter in the oxic wetland environment altering its geochemical signature though time. However, to avoid

potentially biased interpretations related to diagentic alteration of OM in the surficial wetland, and because of a lack of sedimentary material in the upper 6 cm due to root presence, mean values from 9 samples from 6 to 40 cm were used as an end-member in subsequent mixing models (see Fig. 5).

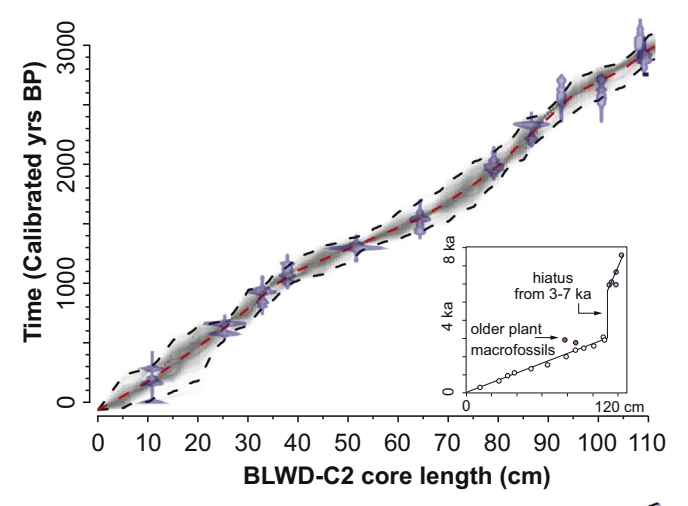
Samples from the base of BLWD-C3 (122 to $136 \, \mathrm{cm}$, n=10) were selected to a represent an endmember of terrestrial organic matter, specifically from a time when *Pinus* was not dominant on the Abaco landscape or elsewhere in the northern Bahamas (pre- $1000 \, \mathrm{cal}$ yr BP, Slayton, 2010; Kjellmark, 1996). The base of BLWD-C3 was notable for its coarse terrestrial organic matter fragments (e.g., leaves, wood fragments, twigs), with negligible fine-grained sedimentary matrix (either organic or inorganic constituents). These sediments were likely deposited during a period of episodic deposition in the sinkhole center.

Cross-plots between $\delta^{15}N_{\rm org}$, $\delta^{13}C_{\rm org}$, and C:N were first used to explore core-based geochemical results and investigate the provenance of organic matter entering Blackwood Sinkhole through time, with respect to (a) modern sinkhole particulate organic matter ($\delta^{13}C_{org}$: -34.5%, mean of n = 6), (b) wetland organic matter ($\delta^{13}C_{org}$: -26.6%, mean of n = 9), and (c) terrestrial organic matter ($\delta^{13}C_{org}$: -26.9%, mean of n=10). These cross-plots do reveal a tripartite division of organic matter sources entering the sinkhole, which is most evident in the crossplot between $\delta^{13}C_{org}$ and C:N (Fig. 6). Previous work has demonstrated that the provenance and relative change in organic matter entering coastal environments through time from specific sources can be estimated using mixing models (Gonneea et al., 2004), when suitable endmembers can be constrained for a given environment. A ternary diagram, or three-endmember mixing model was used to calculate the change in organic matter provenance through time, whereby a specific organic matter sources occupies a corner of the triangle (Dittmar et al., 2001).

Phillips and Koch (2002) presented a set of equations for a two isotope, three end-member mixing model that additionally incorporates relative elemental concentrations (e.g., carbon [C], nitrogen [N]) contributing to the accumulating biomass within a system. This concentration-weighted approach is useful because it takes into account proportional increase of an element (which is assumed, as varied sources are contributing to a system), and eliminates the assumption that the carbon intake from one source is equal to the nitrogen intake from that source (Phillips and Koch, 2002). Although Phillips and Koch (2002) used this approach to differentiate food source contributions to mammalian diets, we employ this methodology to calculate relative source contribution of changing surrounding vegetation and authigenic productivity to the sedimentary organic matter accumulating within a sinkhole system. According to Phillips and Koch (2002), the weighted concentration model will account for large variations of elemental concentrations within the three different contributing sources. Traditionally, $\delta^{13} C_{\rm org}$ and $\delta^{15} N_{\rm org}$ used as the tracers of organic matter to the system and remain the reconstructed terms within a source-contribution mixing model. However, we used $\delta^{13}C_{org}$ and the elemental N:C within the mixing model equation set. The division of organic matter within the system is most strongly evident between the relationship of δ¹³C_{org} and C:N. However, mathematically, Loftis and Meile (2014) suggest that utilizing the N:C ratio as a parameter is necessary in solving for fractional end-member contributions, as both N:C and $\delta^{13}C_{\rm org}$ correspond to the carbon parameter signal. Therefore, with modified equations from Phillips and Koch (2002), mixture contributions can be calculated relative to the organic carbon from three defined endmembers (wetland organic matter (OCw), particulate organic matter (OC_P), and terrestrial organic matter (OC_T)). Goneea et al. (2004) successfully utilized a similar approach in an estuary on the coastal carbonate landscape of the Yucatan Peninsula, Mexico.

End-members within Table 2 and the following equations adopted from Phillips and Koch (2002) were used to calculated the relative fraction of the $\delta^{13}C_{org}$ (ultimately represented by $f_{X, Y, Z}$ (C)) that was sourced by either the named OC_{W_7} OC_{P_7} or OC_{T} end-member. In

Table 1 Radiocarbon	Table 1 Radiocarbon results for all cores.	cores.							
Index No.	Lab number	Core	Core interval (cm)	Material	Conventional ¹⁴ C age	Fraction modern $(\Delta^{14}C)$	$\delta^{13}C_{\mathrm{org}}$ (%0)	Calibrated 1 σ ranges (probability)	Calibrated 2σ ranges (probabability)
1	OS-92769	BLWD-C2	10.5 to 11 cm	Single leaf	205 ± 25	0.975 ± 0.0032	-27.7	0 to 10 (0.1714)	0 to 15 (0.1552)
								150 to 173 (0.4501) 178 to 184 (0.0586)	145 to 214 (0.5482) 267 to 301 (0.2965)
ć	10000	o dinid			-	-	1	273 to 294 (0.3197)	
N	05-92835	BLWD-C2	Z5 t0 Z6 cm	Lear tragments	080 ± 25	0.9188 ± 0.0031	-2/./0	5/0 to 580 (0.26/1) 651 to 670 (0.7328)	563 to 59 (0.3392) 639 to 677 (0.6607)
3	OS-92771	BLWD-C2	32.5 to 33 cm	Leaves	1000 ± 30	0.8828 ± 0.0032	-27.7	834 to 841 (0.0707)	798 to 815 (0.0601)
								909 to 958 (0.9293)	822 to 869 (0.1997) 898 to 967 (0.7401)
4	OS-90975	BLWD-C2	37.5 to 38 cm	Twig	1160 ± 25		-27.24	1007 to 1029 (0.2186)	983 to 1034 (0.2638)
								1053 to 1092 (0.4764)	1048 to 1151 (0.6654)
								1106 to 1136 (0.2632) 1162 to 1167 (0.0417)	1156 to 1171 (0.0706)
2	92606-SO	BLWD-C2	51.25 to 51.75 cm	Twig	1380 ± 25		-27.58	1286 to 1307 (1.)	1277 to 1336 (1.)
9	OS-90995	BLWD-C2	64 to 64.5 cm	Twig		0.8166 ± 0.0032	-27.21	1420 to 1434 (0.1037)	1415 to 1572 (0.9473)
								1440 to 1461 (0.1864) 1513 to 1563 (0.7097)	1581 to 1602 (0.0526)
7	OS-89451	BLWD-C2	77.5 to 78 cm	Leaf	2780 ± 35		-28.88	2810 to 2813 (0.0273)	2787 to 2957 (1.)
								2845 to 2929 (0.9102)	
œ	22-909-SO	BI.WD-C2	78.75 to 79.25 cm	Twio	2030 + 25		-29.1	2530 (0 2543 (0.0024) 1934 to 1937 (0.0254)	1899 to 1912 (0.0225)
ò				0	I			1945 to 2003 (0.9413)	1921 to 2059 (0.9752)
								2029 to 2033 (0.0332)	2099 to 2101 (0.0021)
6	8Z606-SO	BLWD-C2	86 to 86.5 cm	Twig	2610 ± 35		-27.55	2729 to 2760 (1.)	2551 to 2555 (0.0034)
									2618 to 2633 (0.03082)
Ç	1								2705 to 2787 (0.9657)
10	OS-92771	BLWD-CZ	86 to 87 cm	Twigs	2290 ± 25	0.752 ± 0.0023		2313 to 2347 (1.)	2183 to 2234 (0.2192) 2306 to 2350 (0.7807)
11	OS-92772	BLWD-C2	92 to 93 cm	Twigs	2400 ± 30	0.7412 ± 0.0026		2353 to 2376 (0.2327)	2346 to 2493 (0.9030)
								2384 to 2459 (0.7672)	
;			1				1		2640 to 2680 (0.0852)
12	OS-90994	BLWD-C2	100 to 101 cm	Twig	2520 ± 35	0.7303 ± 0.0032	-15.79	2503 to 2530 (0.1661) 2537 to 2594 (0.4102) 2614 to 2637 (0.1844) 2696 to 2727 (0.2301)	2487 to 2742 (1.)
13	96606-80	BIWD-C2	108 to 108 5 cm	Twio	2890 + 35	0.6974 + 0.0027	-17 29	3072	2891 to 2903 (0.01395)
				0	ı	ı	Ì		2924 to 3084 (0.8392)
7	0.00	CO CLIMIC	100 75 42 100 95	Ë	+		1	0000 0000 0000	3086 to 3159 (0.1467)
14 1	02-89430	DLWD-C2	108.75 to 109.25cm	1 W IS	2/90 ± 30		-17.39	2633 [0 2928 (0.9729)	2/94 to 2831 (0.0910)
15	OS-121884	BLWD-C3	42 cm	Leaf	350 ± 30	0.9576 ± 0.0017	-26.94	319 to 392 (0.593)	308 to 498 (1.)
7	100101	C) CIMIN	09 04 29	J I	+		00	426 to 476 (0.407)	(027 0) 600 54 162
01	03-121003	DLWD-C3	0/ 10 00 CIII	real	06 ± 500	0.0010 ± 6.0010	- 29.29	/ 40 to / 98 (0.701) 870 to 898 (0.299)	/31 t0 833 (0.8/2) 844 to 908 (0.328)
17	OS-121886	BLWD-C3	81 to 82cm	Leaf	1200 ± 30	0.8618 ± 0.0018	-18.6	1079 to 1162 (0.943)	1010 to 1021 (0.014)
								1171 to 1176 (0.057)	1055 to 1185 0.925)
18	08-121887	BI WD-C3	109 cm	Twies	1520 + 30	0.8275 + 0.0016	-26.25	1354 to 1415 (0 827)	1207 to 1235 (0.061) 1341 to 1424 (0.657)
2	00171-00		10.01	1 11 153	1	1	9	1464 to 1477 (0.111)	1428 to 1444 (0.034)
								1505 to 1513 (0.062)	1415 to 1522 (0.309)
19	OS-121888	BLWD-C3	122 cm	Leaf	1620 ± 30	0.8170 ± 0.0016	-18.51	1420 to 1459 (0.417)	1412 to 1568 (0.999)
20	OS-113156	BLWD-C6	108 to 109.5 cm	Twig	1490 ± 20	0.8305 ± 0.0026	-27	1351 to 1390 (1.)	1389 to 1591 (0.001) 1330 to 1409 (1.)



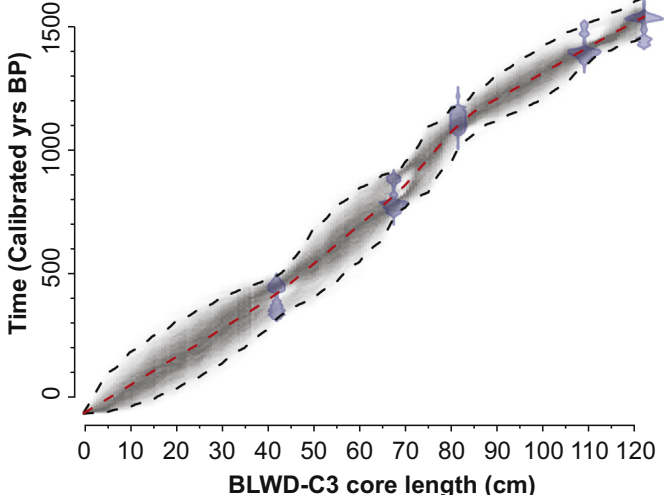


Fig. 3. Downcore age models for BLWD-C2 (inset in top depicts likely depositional hiatus) and BLWD-C3 (bottom).

addition, the equations below were translated into both R and Python scripts for use by other researchers in similar applications. The scripts can be located at https://github.com/sergey-molodtsov/end_member.

Eq. (1): Mass balance equation for $\delta^{13}C_{org.}$ $\delta^{13}C_{org}$ is representative of the modeled bulk carbon isotopic signature of the mixture (or sample interval downcore), $f_{X,C}$, $f_{Y,C}$, $f_{Z,C}$ are the fractional contributions calculated for C. $\delta^{13}C_X$, $\delta^{13}C_Y$, $\delta^{13}C_Z$ are the $\delta^{13}C_{org}$ of the selected endmembers (OC_W: X, OC_P: Y,OC_T: Z), respectively.

$$\delta^{13}C_{m} = f_{X,C}\delta^{13}C_{X} + f_{Y,C}\delta^{13}C_{Y} + f_{Z,C}\delta^{13}C_{Z}$$
(1)

Eqs. (2)–(4): Sum of the fractions for $\delta^{13}C_{org}$ (f_{X,Y,Z (C)}, f_{X,Y,Z (N)}), and accumulated biomass (f_{X,Y,Z (B)}).

$$1 = f_{X,C} + f_{Y,C} + f_{Z,C}$$
 (2)

$$1 = f_{X,N} + f_{Y,N} + f_{Z,N}$$
 (3)

$$1 = f_{X,B} + f_{Y,B} + f_{Z,B}$$
 (4)

Eqs. (5)–(8): Phillips and Koch (2002) published matrix notation to solve for combining the system of linear equations necessary for calculating the fraction of assimilated biomass ($f_{X,B}$, $f_{Y,B}$, $f_{Z,B}$) within a mixture interval.

$$AF = B (F = A^{-1}B)$$

$$(5)$$

$$A = \begin{bmatrix} (\delta^{13}C_{x} - \delta^{13}C_{m})_{[C_{X}]} & (\delta^{13}C_{Y} - \delta^{13}C_{m})_{[C_{Y}]} & (\delta^{13}C_{z} - \delta^{13}C_{m})_{[C_{Z}]} \\ (N: C - N: C_{m})_{[C_{X}]} & (N: C_{Y} - N: C_{m})_{[C_{Y}]} & (N: C_{Z} - N: C_{m})_{[C_{Z}]} \\ 1 & 1 & 1 \end{bmatrix}$$

$$(6)$$

$$F = \begin{bmatrix} f_{X,B} \\ f_{Y,B} \\ f_{Z,B} \end{bmatrix} \tag{7}$$

$$B = \begin{bmatrix} 0 \\ 0 \\ 1 \end{bmatrix} \tag{8}$$

Eqs. (9)–(11): $f_{X,C}$, $f_{Y,C}$, $f_{Z,C}$ represent the fractional contributions of the calculated assimilated biomass ($f_{X,B}$, $f_{Y,B}$, $f_{Z,B}$) relative to the C and N concentrations within end-member selected values.

$$f_{X,C} = \frac{f_{X,B}[C]_X}{f_{X,B}[C]_X + f_{X,B}[C]_Y + f_{X,B}[C]_z}$$
(9)

$$f_{Y,C} = \frac{f_{Y,B}[C]_Y}{f_{X,B}[C]_X + f_{X,B}[C]_Y + f_{X,B}[C]_z}$$
(10)

$$f_{Z,C} = \frac{f_{Z,B}[C]_Z}{f_{X,B}[C]_x + f_{X,B}[C]_y + f_{X,B}[C]_z}$$
(11)

The selected end-members can successfully estimate the organic matter provenance for approximately 56% of the data from BLWD-C2 and BLWD-C3. For the remaining 44% of the data, modeled estimates of organic matter sources had one of the tripartite sources either below 0% or above 100%. Such intervals were interpreted as representing the extremities of the end-member source contributions. For example, intervals that documented fractions ($f_{X,C}$, $f_{Y,C}$, $f_{Z,C}$) < 1 (i.e., negligible contribution from that particular source end-member) were forced to 0, while intervals that documented fractions > 1 (i.e., significant contribution from that particular source end-member) were forced to 1.

To test the assumption that only 3 endmembers explain the dataset, the $\delta^{13}C_{org}$ was back-calculated by using: (a) the fractional output of organic matter sources the original model run, modified by forcing excessive values to either 0 or 100%, and (b) the endmembers used. The resultant calculated $\delta^{13}C_{org}$ values were highly correlated to the originally measured $\delta^{13}C_{org}$ values ($r^2=0.84$, with $p<0.0.05,\,n=218$). This indicates that the model tends to underestimate the measured concentrations of $\delta^{13}C_{org}$, especially for enriched values. Perhaps this is related to an under representation of ocean-derived OC_P delivered to the sinkhole during high-intensity events (e.g., hurricanes, see crossplot in Fig. 6), but in general, the model capture the overall geochemical trends.

5. Results

5.1. Lithology

The sinkhole cores terminate on a carbonate gravel deposit (pebbles to cobbles), above which is either terrestrial plant macrofossils or laminated algal sapropel (i.e., gyttja) interbedded with layers of increased calcium carbonate. In addition, the sapropel matrix was interspaced by horizons of increased coarse-grained particles. Lamination thickness varied from the µm-scale to mm-scale, and alternated between horizons rich in calcium carbonate versus organic matter. There is no evidence of bioturbation evident within the cores, likely from the benthic anoxia. The cores are generally devoid of shell material, except occasional brackish water bivalves (i.e., pea clams) that are likely displaced from micro-habitat along the vertical sinkhole wall flooded by the upper meteoric lens or adjacent wetland. Other than the striking laminations, the most salient sedimentary feature is a prominent horizon of non-laminated sapropel containing no coarse-grained particles

Table 2 End-member values for sinkhole particular organic matter, and wetland/terrestrial organic matter.

End-member	Site	GPS location	Salinity (psu)	δ $^{13}C_{org~(\%)}$	N:C
Sinkhole particulate	Treasure Cay		0.88	-36.2	0.10
Organic matter	Emerald Pond	26.536°, -77.108°	1.30	-33.2	0.08
	Blackwood	26.798°, -77.423°	1.79	-37.6	0.12
	Great Cistern	26.570°, -77.118°	5.48	-33.0	0.15
	Sawmill Sink	26.217°, -77.210°	0.86	-32.0	0.09
	Lost Reel		0.66	-35.1	0.12
	Mean $(n = 6) \pm 1 \sigma$		1.83	-34.5 ± 2.5	0.11 ± 0.02
Wetland	BLWD-C6, 6-8 cm	26.799°, -77.422°		-27.2	0.07
Organic matter	BLWD-C6, 8-10 cm			-26.8	0.06
	BLWD-C6, 14-16 cm			-27.1	0.06
	BLWD-C6, 24-26 cm			-26.4	0.05
	BLWD C6, 26-28 cm			-26.3	0.05
	BLWD C6, 28-30 cm			-26.2	0.05
	BLWD C6, 32-34 cm			-26.3	0.06
	BLWD C6, 36-38 cm			-26.4	0.04
	BLWD C6, 40-42 cm			-26.8	0.04
	Mean $(n = 9, 6-40 \text{ cm}) \pm 1 \sigma$			-26.6 ± 0.4	0.05 ± 0.01
Terrestrial	BLWD-C3, 122-123 cm	26.798°, -77.423°		-29.0	0.03
Organic matter	BLWD-C3, 123-124 cm			-29.0	0.03
	BLWD-C3, 124-125 cm			-28.2	0.02
	BLWD-C3, 125-126 cm			-26.7	0.01
	BLWD-C3, 126-127 cm			-26.3	0.01
	BLWD-C3, 127-128 cm			-25.1	0.02
	BLWD C3, 128-129 cm			-26.4	0.02
	BLWD-C3, 129-130 cm			-26.5	0.02
	BLWD-C3, 130-131 cm			-26.1	0.02
	BLWD-C3, 131-132 cm			-25.6	0.02
	Mean $(n = 10, 122-131) \pm 1 \sigma$			-26.9 ± 1.3	0.02 ± 0.01

that can be correlated between cores, and which occurs from 10 to 16 cm (median age: \sim 371–158 cal yr BP) in core 2, and from 25 to 31 cm depth in core 3 (median age: \sim 291–223 cal yr BP).

5.2. Age models and sedimentation rates

The benthic sinkhole periphery (BLWD-C2) was likely characterized by episodic sedimentation from 109 to 122 cm, which equates to 7622 to 7494 cal yr BP₁₉₅₀ (2 σ , 0.99 probability) until 2960 to 2838 cal yr BP (2 σ , 0.91 probability). Afterwards, the sedimentation rate was nearly constant through the late Holocene (3000 years to present) from 109 to 0 cm (least squares linear regression: $r^2 = 0.99$, n = 11 dates, 0.3 to 0.6 mm yr⁻¹). Since sediment was sampled at every-other 5 mm interval downcore, each sample represents 16 to 32 years, providing a multi-decadal late Holocene geochemical record from BLWD-C2.

The sinkhole center (BLWD-C3) had an age of 1412 to 1568 cal yr BP (2 σ , 0.99) at 122 cm depth. This means that the sedimentation rate in the sinkhole center doubled that along the periphery (BLWD-C2), but only during the last ~1500 years. If one includes the year of core collection in 2013, a simple linear model describes the age-depth relationship between the radiocarbon dates using the midpoint of the highest probability calibrated 2 σ result (least squares linear regression: $r^2 = 0.99$, n = 6, ~1.2 mm yr $^{-1}$). Since sediment was sampled at continuous 10 mm intervals downcore, each sample represents ~8.3 years down core, providing an approximately decadal geochemical record from BLWD-C3.

Geochemical and sedimentary results from below 122 cm in core 3 (\sim 1540 cal yr BP) and below 110 cm in core 2 (\sim 2800 cal yr BP) are not plotted age-wise because of poor age control, the potential for episodic sedimentation, and sedimentary evidence for basal condensed horizons (discussed below).

5.3. Isotopic and geochemical signals preserved in bulk organic matter

Similar downcore trends are observed in the geochemical signatures from BLWD-C2 and BLWD-C3. In general, a similar range of $\delta^{13}C_{\rm org}$ values between these cores indicates consistent organic matter source

deposition whether in the center or periphery of the sinkhole. However, the $\delta^{15}N_{\rm org}$ value of organic matter deposited in the sinkhole center (BLWD-C2) is slightly more depleted than along the periphery (BLWD-C3). The model assumes that only three sources of organic matter were supplied to Blackwood Sinkhole over the last 3000 years based on the ternary model between $\delta^{13}C_{\rm org}$ and N:C. The mixing model suggests that the dominant organic matter source fluxed to the sinkhole can be summarized as primarily OC_T from ~3000 to ~1500 cal yr BP, OC_P from ~1500 to ~1000 cal yr BP, and OC_W from ~1000 cal yr to present (Fig. 7).

The oldest part of the record dates from ~3000 to ~1500 cal yr BP, and is only represented in BLWD-C2. The mean $\delta^{15}N_{org}$ values are ~3‰, C:N ~30, and $\delta^{13}C_{org}$ values oscillate around -31%. The values of $\delta^{13}C_{org}$ and C:N align with previously published values of terrestrial vegetation and aquatic productivity sources (O'Leary, 1988; Keeley and Sandquist, 1992; Meyers, 1994; Lamb et al., 2006). Mean C:N values are highest within this interval, and by comparison with published values of C:N, $\delta^{15}N_{org}$ and $\delta^{13}C_{org}$, high C:N values are consistent with organic matter primarily derived from terrestrial plants (Thornton and McManus, 1994; Ogrinc et al., 2005; Lamb et al., 2006 and references therein). During this interval, there is a dominant > 75% calculated OC_T contributing to the organic matter within the sinkhole. However, this interval also shows marked contributions from OC_P.

A dominant OC_T (> 75%) contribution begins to diminish at ~1500 cal yr BP-present to approximately ~30%, with episodic fluctuations of up to 60% (Fig. 7). From ~1500 to ~1000 cal yr BP, the $\delta^{15}N_{org}$ value oscillates from 3 to 6‰ and the $\delta^{13}C_{org}$ value oscillates from -35 to -28‰, which is consistent with literature values representing freshwater algae in lake zones (France, 1995). There is an approximate 80% increase in OC_P (%) flux to the benthos during this interval.

From \sim 1000 cal yr BP to present, the $\delta^{15}N_{org}$ value oscillates from 0 to 2‰ and the $\delta^{13}C_{org}$ value oscillates from -29 to -26‰. The $\delta^{13}C_{org}$ and $\delta^{15}N_{org}$ values and C:N ratio signatures fall within accepted values for other mangrove and wetland species abundant in similar marginal marine environments (including those fringed with *Rhizophora*, which is abundant within the Caribbean) (Gonneea et al., 2004; Larsen et al.,

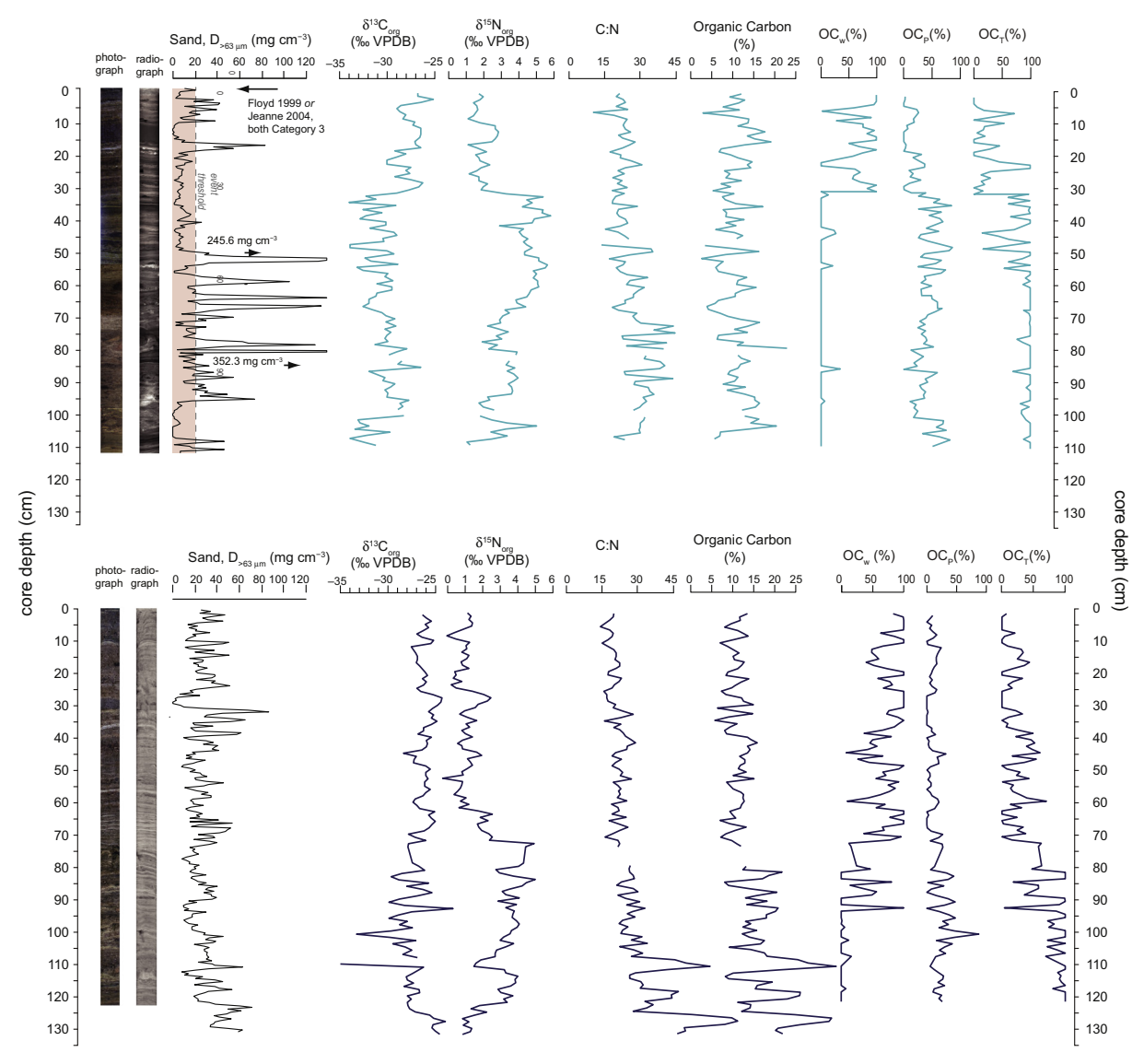


Fig. 4. Core photographs, X-radiographs, sand content, and bulk organic matter geochemistry, including the deposition of the three primary sources of organic matter based on 3-endmember mixing models for BLWD C2 (top), and BLWD C3 (bottom).

2012). There is an approximate > 80% increase in OC_W contributing to the organic matter during this time interval. There are notable fluctuations of depleted $\delta^{13}C_{\rm org}$ (approximately $\sim 3\%$) at 770–550, and 300–100 cal yr BP, corresponding to increases of OC_P % (approximately 30–40%) and OC_T % (approximately 60%) contributions.

6. Discussion

6.1. Deposition prior to 3000 cal yr BP

Neither sinkhole core preserves a significant sedimentary record prior to 3000 cal yr BP. During the early and middle Holocene when relative sea level and local groundwater level were lower, it is possible that organic matter and other sediments were exported into the lower cave chamber (The Pit, Fig. 2). In Hoyo Negro in Mexico, which has very similar conduit geometric relationships to Blackwood Sinkhole, Collins et al. (2015a) documented that during lower water levels of the early Holocene sediment bypassed shallower conduits and instead accumulated in deeper depocenters. It is possible that a similar process impacted Blackwood Sinkhole, and indeed, divers have observed detrital peat deposits in The Pit adjacent to Blackwood Sinkhole (Brian Kakuk, personal communication). From 7000 to 3000 cal yr BP, some

organic sediment began accumulating in Blackwood along the sinkhole periphery at the site of core 2, and the base of core 3 has a condensed horizon of wood fragments. However, this deposition appears episodic and continuous deposition does not begin at the base of Blackwood Sinkhole during the late Holocene.

6.2. Lateral changes in inorganic coarse particle deposition

Lateral changes in coarse particle deposition were observed between the sinkhole periphery and center. For example, horizons with coarser particles were more common in the sinkhole periphery (BLWD-C2). The coarse particles were weathered and friable inorganic fragments of limestone, and also biologic remains such small bivalves (e.g., pea clams). These coarse particles were often associated with horizons of fine grained calcium carbonate (see Fig. 2 in van Hengstum et al., 2016), perhaps suggesting a linkage between intense rain events and fine-grained carbonate deposition in the basin. The mean grain size of deposited particles was not measured, but karst fragments that were 0.5 to 1 cm in diameter were frequently preserved in BLWD-C2 (van Hengstum et al., 2016). No such particles were observed in BLWD-C3. Previous analysis of sediment 220 m away on the beach documented abundant tests of marine benthic foraminifera (e.g., *Archaias*) in the

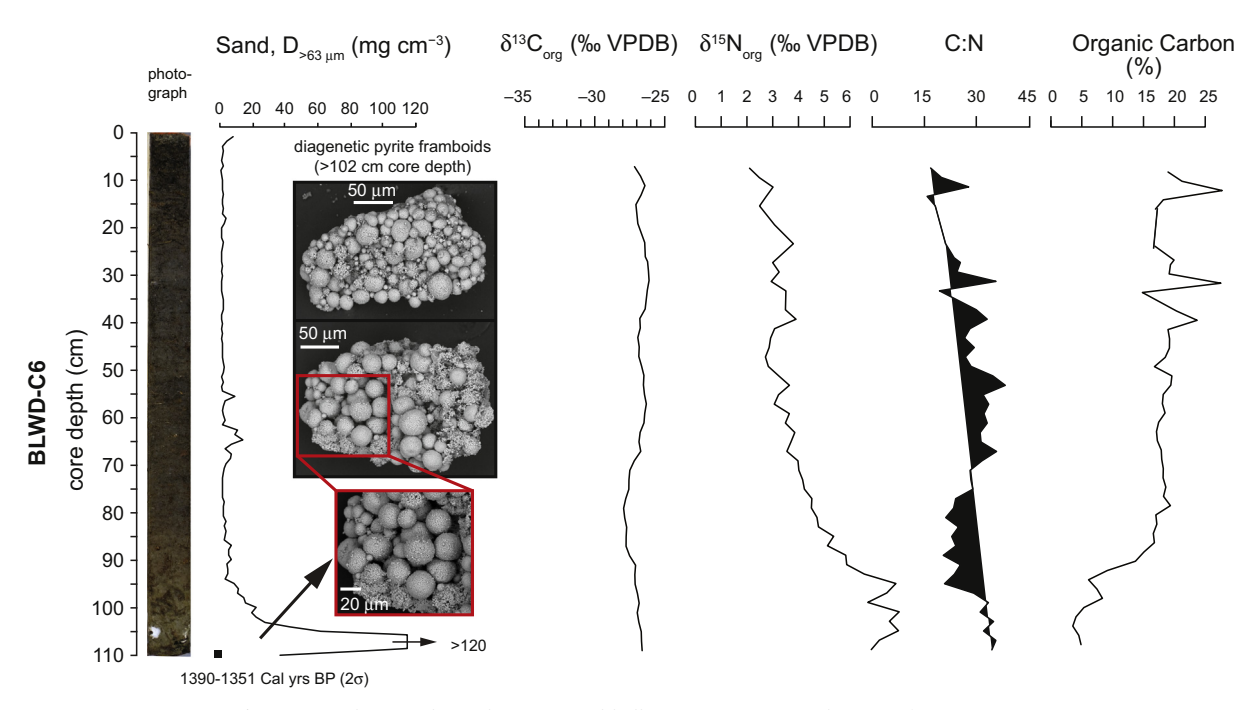


Fig. 5. Core photograph, sand content, and bulk organic matter geochemistry for BLWD-C6.

sand (van Hengstum et al., 2016), which were not observed in the coarse horizons. More broadly, this suggests that any sediment eroding into the basin was located within a 220 m radius (proximal source) or within the basin itself.

More quantitatively, the background coarse particle deposition in BLWD-C2, or the abundance of sedimentary particles coarser than 63 μm (D $_{>63\mu m}$), was generally $<10\,mg\,cm^{-3}$. Only during times of intense landscape flooding related to hurricanes did coarse particle

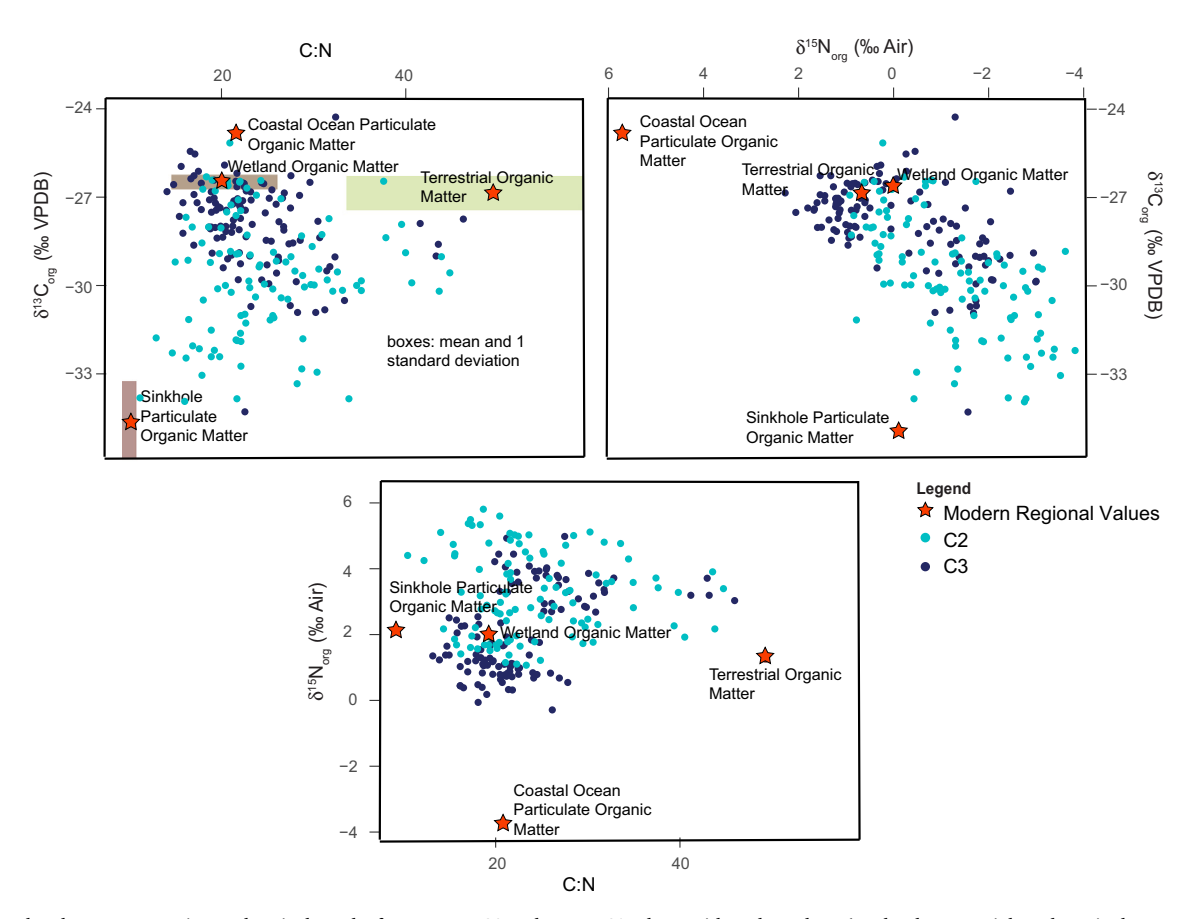


Fig. 6. Cross-plots between organic geochemical results from BLWD-C2 and BLWD-C3, along with endmembers (wetland, terrestrial, and particulate organic matter) and modern isotopic values (e.g., ocean particulate organic matter).

Time (Calibrated yrs BP)

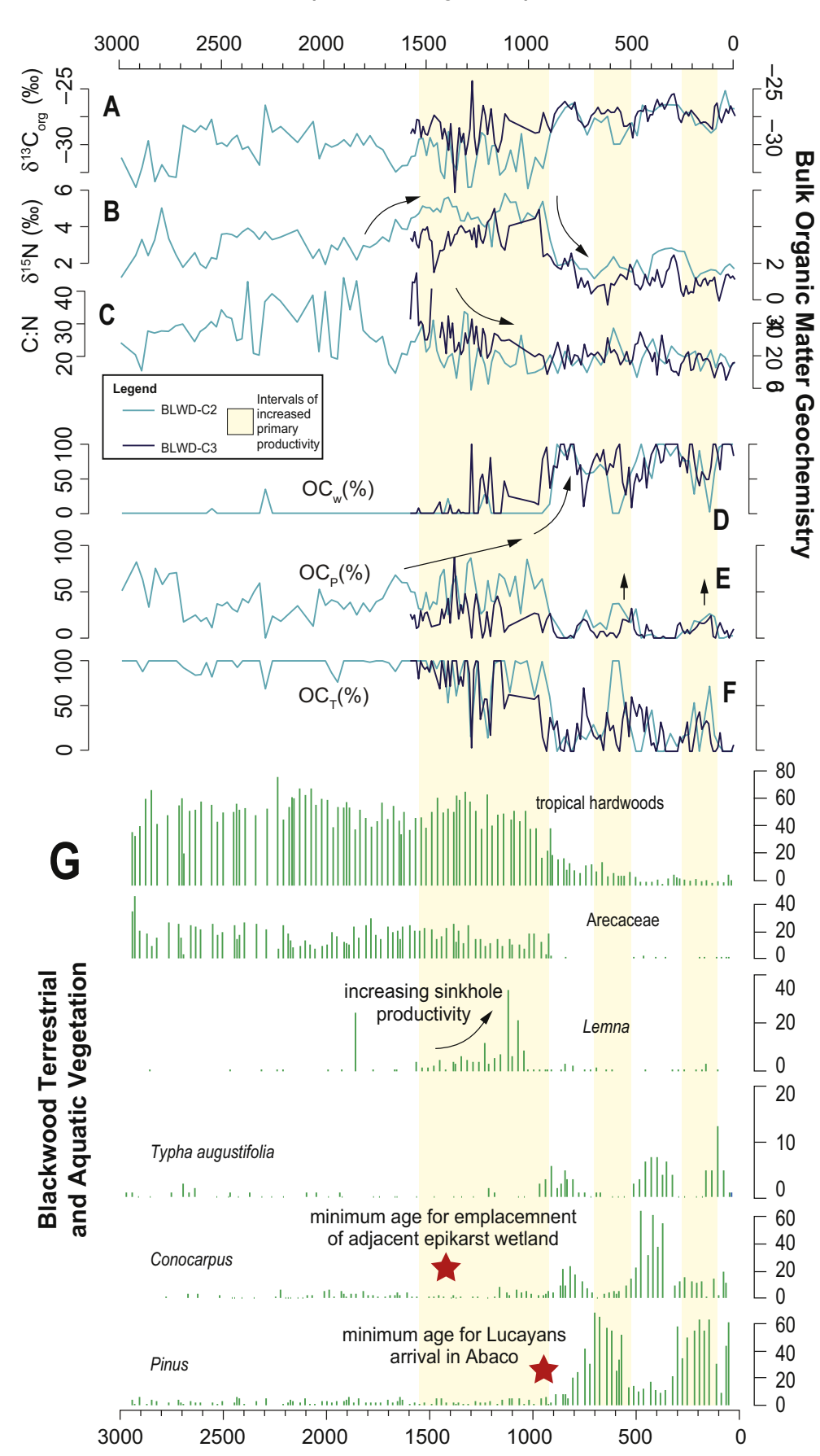


Fig. 7. Comparison of geochemical results from BLWD-C2 and BLWD-C3 to regional climate and vegetation signals, 0 is 2000 CE. (A-B) Age-wise trends in $\delta^3 C_{org}$, $\delta^{15}N$, and C:N, (D-F) Age-wise variability in wetland organic matter (OC_W), particulate organic matter (OC_P), and terrestrial organic matter (OC_T), and (G) dominant pollen preserved in BLWD-C3.

deposition exceeded 20 mg cm $^{-3}$ (50 to 352 mg cm $^{-3}$), especially during the interval from $\sim\!1300$ to 2600 cal yr BP (van Hengstum et al., 2016). For example, the most recent increase in coarse particle deposition in BLWD-C2 is within dating uncertainties of either Hurricane Floyd (1999) or Hurricane Jeanne (2003) (van Hengstum et al., 2016). In contrast, deposition of coarse particles was generally higher in BLWD-C3, with a background deposition of D $_{>63\mu m}$ of 20 to 30 mg cm $^{-3}$. Rarely did coarse particle deposition exceed 40 mg cm $^{-3}$ in BLWD-C3, and, unfortunately, there is negligible sediment record in BLWD-C2 older than 1300 cal yr BP for comparison to BLWD-C2.

This apparent sorting of particles can be explained by simple advective settling, whereby during intense hurricane events the largest particles are preferentially deposited proximal to a physical barrier that causes a decrease in water velocities at depth, and therefore decreases the water's transport competency (Woodruff et al., 2008). In the case of Blackwood Sinkhole, this physical barrier is the structural edge of the sinkhole. We speculate that ongoing wind action likely elevates background coarse particle deposition in the sinkhole center (BLWD-C3) versus periphery (BLWD-C2).

The core from the adjacent wetland (BLWD-C6) only contains peat with no evidence of sedimentary particles derived from the adjacent beach. Given the proximity of the shorelines to the site of BLWD-C6, the lack of any beach sediment accumulating in the wetland suggests conditions not locally favorable for its preservation (i.e., acidic). In general, coarse particle deposition was low (D $_{>\,63\mu m}$ of 1 to 3 mg cm⁻³), but the lowermost section (100-110 cm) contains increased coarse particles content (D $_{>63\mu m}$ exceeds 60 mg cm⁻³). This interval also coincides with a slight color change to lighter-hued peat with increased fine-grained sedimentary matrix. Scanning electron microscopy indicates these coarse particles are pyrite frambiod aggregates up to 20 µm in diameter, which are likely pore water precipitates related to early diagenesis (Taylor and Macquaker, 2000). A radiocarbon sample from the base of core 6 (BLWD-MC1 in van Hengstum et al., 2016) was dated to 1330 to 1409 cal yr BP (20, 1.0 probability, Table 1), which is the deepest peat deposits mapped from this area. This provides a minimum age for emplacement of the wetland adjacent to Blackwood Sinkhole (Fig. 1). The presence of pyrite framboids at the basal stratigraphic interval of BLWD-C6 suggests an increase in aerial coverage of wetland vegetation on the landscape, likely due to a transgression of sea level (Brown and Cohen, 1995).

6.3. Large-scale changes in OM provenance at 1500 and 1000 cal yr BP

Bulk organic matter was dominated by OC_T sources from 3000 to \sim 1500 cal yr BP (> 80%), based on BLWD-C2 (Fig. 7). One may hypothesize that this increased OC_T delivery may be related to hurricane activity alone. However, the western North Atlantic margin experienced increased intense hurricane activity (category ≥3, Saffir-Simpson Scale) from 2600 to 1000 cal yr BP (Donnelly and Woodruff, 2007; van Hengstum et al., 2016), suggesting additional factors are influencing sediment delivery into the sinkhole. Deposition of organic matter along the sinkhole periphery was perhaps favored over the center of the basin by advective settling, similar to the accumulation of coarse inorganic particles. On the adjacent terrestrial landscape, the pollen record from BLWD-C2 indicates that tropical hardwoods (e.g., Myrtaceae) and palms (Arecaceae) dominated the forest community (Fig. 7G). A similar result was obtained based on a pollen record from another Abaconian karst basin (Emerald Pond; Slayton, 2010). These plant species would have provided an adequate supply of OC_T with a requisite stable carbon isotopic ratio for erosion into Blackwood Sinkhole.

The ternary model indicates that negligible OC_W was transported into the sinkhole from 3000 to 1500 cal yr BP, which suggests that there was limited wetland development on the adjacent epikarst surface. In addition, the high C:N ratios preserved in the sedimentary record suggest that terrestrially-derived organic matter fluxing into the sinkhole was minimally degraded. Some uncertainty may result from some vascular plants having a similar $\delta^{13}C_{org}$ value as wetland plants, which may have biased the results of the mixing model. However, the geochemical result is consistent with the pollen preserved in BLWD-C2, which documents negligible wetland taxa during this time (Fig. 7G). We note that minimal relative sea-level change occurred in the Bahamas during the late Holocene (Khan et al., 2015), so the absence of wetlands on the epikarst surface at this time is curious. It may have been possible that wetlands were hampered on the epikarst surface prior to 1000 cal yr BP during the period of intense regional hurricane activity.

At 1500 cal yr BP, a constant (i.e., linear) sedimentation rate was initiated in the center of the basin (BLWD-C3: \sim 1.2 mm yr $^{-1}$) that doubled sedimentation rates around the periphery of the periphery (BLWD-C2: \sim 0.3 to 0.6 mm yr $^{-1}$). Based on a minimum age from the core in the adjacent wetland (BLWD-C6), wetland environments became established on the adjacent epikarst surface by \sim 1400 cal yr BP (Fig. 1D, Table 1), which no doubt began influencing sedimentation and environmental conditions in the sinkhole. Indeed, the increased sedimentation rate alone in BLWD-C3 indicates elevated sedimentary flux from the wetland. However, the geochemical ternary model also estimates OC_W fluctuations to > 80% archived in BLWD-C3 (Fig. 7F). This demonstrates the success of wetlands on the adjacent epikarst surface at providing a competent sediment flux to karst basins in the Bahamas, as has been similarly observed on the Yucatan Peninsula (Collins et al., 2015b).

From 1500 to 1000 cal yr BP, the flux of OC_P to the benthos along the periphery of Blackwood Sinkhole increased and remained above 50% (BLWD-C2, Fig. 7E). The sinkhole walls do provide ecospace that can be colonized by benthic primary producers, which likely is increasing the OC_P flux to the sinkhole periphery relative to the center. However, the abrupt change in OC_P sedimentation at 1000 cal yr BP is unlikely related to change in the surface of this vertical habitat relative cause by sea-level change because rates of relative sea-level rise have been minimal over the last 2000 years (Khan et al., 2015).

This period also coincides with an increase in Lemna (duckweed) in the pollen record, which is a free-floating aquatic plant (Fig. 7G). The combined increase in OC_P and \emph{Lemna} points toward an increase in nutrients and primary productivity in the water column, coincident with the installation of the wetland on the adjacent epikarst surface at \sim 1300 cal yr BP. This suggests an additional role of the wetland whereby it enhanced primary productivity in the sinkhole basin, perhaps through a subaerial flux of particles and OC_W. Increased primary productivity from more eutrophic conditions within the sinkhole could progressively fractionate the residual dissolved inorganic nitrogen (DIN) pool in the sinkhole (Talbot and Laerdal, 2000; Brandenberger et al., 2011). This process could have potentially enriched the nitrogen isotopic ratio of the subsequently produced OC_P from 1500 to 1000 cal yr BP. Given that the upper portion of the aquifer is the meteoric lens (ML, Fig. 1D), which is constantly discharging at the nearby coastline (Fig. 1D), it remains uncertain whether this increased productivity was driven by a local increase in nutrient residence time or concentration, in response to some broader hydroclimate change (ocean-atmospheric cause) or just the adjacent wetland (local cause). However, the wetland itself must not be the sole driver of the OC_P flux to the benthos since additional OC_P oscillations occur from 1500 cal yr BP to present when the adjacent wetland is assumingly most developed.

The final most prominent geochemical trend is the shift to > 80% OC_W deposition from 1000 cal yr BP to the present at both core sites, and decreased contribution from OCP and OCT. The pollen record indicates that this shift also coincides with a significant decrease in tropical hardwoods and palms (Arecaceae) and increase in wetland taxa on the adjacent landscape (e.g., Conocarpus, Typha augustifolia). Elsewhere, Collins et al. (2015b) noted that sedimentation in an anchialine cave in Mexico (Yax Chen) increased when mangroves colonized the adjacent epikarst surface from inundation by Holocene sea-level rise. A similar process has impacted Blackwood Sinkhole as indicated by the pollen and geochemical records, whereby colonization of wetlands on the adjacent epikarst surface by ~1300 cal yr BP first initiated sedimentation on the subaerial topographic depression. At Blackwood Sinkhole, however, enhanced sedimentation of OCw is slightly delayed until 1000 cal yr BP, perhaps due to local hurricane activity (suppressing tree development) or regional hydroclimate variability. This final period of wetland expansion during the last millennia on Abaco also coincides with pine forests colonizing the Abaco landscape (at ~700 cal yr BP; van Hengstum et al., 2016), with a concomitant loss in the dominance of tropical hardwoods and palms (Arecaceae).

The last 1000 years are known as a period of considerable change in the Caribbean region with humans continually modifying the landscape, and evidence of regional hydroclimatic change resulting from northern hemisphere cooling during Little Ice Age. However, the relative role of humans versus hydroclimate (seasonality, direction and magnitude) on a regional scale remains uncertain. On nearby Andros, a coeval increase in *Pinus* on the landscape in the last ~700 years has also been documented like on Abaco (Kjellmark, 1996), which some may argue is caused by Native Lucayan activities. Only in the northern Bahamian islands is Pinus significantly present on the landscape (Grand Bahama, Abaco, Andros, New Providence). As previously discussed, the sources of allochthonous sedimentary organic matter (OC_W, OC_T) in Blackwood are from a ~220 m radius of the site, with internal hydrographic conditions and nutrient concentrations likely impacting OC_P sedimentation. Therefore, sedimentary organic matter quality and quantity become a proxy for water column conditions that are necessarily linked to regional rainfall either by changing the dissolved or particulate flux of nutrients. In addition, centennial-scale correlations between flora (terrestrial and wetland) in the pollen record and OC_P can be drawn during the last 1000 years in Blackwood Sinkhole. For example, decreased wetland taxa (e.g., Conocarpus and Typha augustifolia) correspond with increased OCP%, OCT %, and Pinus on the landscape (e.g., 550-700, and 100 to 300 cal yr BP). However, resolving the magnitude, direction, or annual timing of rainfall delivery (i.e., seasonality) remains uncertain based on the OC_P percentage change alone.

On Holocene timescales, Caribbean rainfall is linked to solar insolation (Hodell et al., 2001), but the drivers of regional rainfall on shorter times scales are complex and still under investigation (e.g., Fritz et al., 2011.). Based on factor analysis of modern precipitation data, Jury et al. (2007) group both the northwestern region of Cuba, the Little Bahama Bank and the Great Bahama Bank in the same Caribbean precipitation zone. This suggests that these areas should have experienced a similar hydroclimate change in recent time. Isotopic results on northwestern Cuban speleothems suggest either an abrupt shift to increased precipitation at 1000 years ago (Fensterer et al., 2013) or a long-term increase in precipitation over the last 1000 years (Fensterer et al., 2012). In contrast, trace metal runoff proxies in a coastal lagoon from northwestern Cuba suggest drying over the last 1000 years (Gregory et al., 2015). On nearby Florida, a pollen record from Lake Tulane (~400 km to the west of Blackwood Sinkhole, closer than Cuba) pointing to the expansion of pines during the last 5000 years and during previous Heinrich Events, is ascribed increased regional moisture (Grimm et al., 2006). Clearly, additional records are needed from the northern Caribbean to understand the regional hydroclimate changes over the last millennium, and fully understand how rainfall impacted primary productivity in Blackwood Sinkhole.

Nutrient availability in the water column within a groundwater-fed carbonate sinkhole is complex and not yet fully understood. However, both oligotropic and eutrophic conditions are known from tropical karst basins. Assuming that similar hydrogeological forcing conditions also operated in the past and that these are real features of the local sedimentary dynamics, a change in primary productivity potentially suggests: (a) changing nutrient residence time in the sinkhole, or (b) changing nutrient delivery to, or concentration within the sinkhole water column. Both changing nutrient residence time in the sinkhole and changing nutrient delivery within the water column could be due to variations in regional rainfall. It appears worthwhile to further examine the drivers of primary productivity in karst basins to better resolve the climatic significance of the OC_P signal archived in terrestrial karst basins, especially considering the isotopic variability of algal biomarkers in karst basin sediment records are useful hydroclimate proxies (Richey and Sachs, 2016).

7. Conclusions

- During the late Holocene (3000 cal yr BP to present), Blackwood Sinkhole on Great Abaco Island in The Bahamas received organic matter supplied from three primary sources: wetland organic matter from the adjacent epikarst surface, autochthonous primary productivity in the upper meteoric lens (oligohaline salinity), and terrestrial organic matter from the surrounding landscape.
- Based on a three-endmember mixing model using $\delta^{13}C_{org}$ and N:C, the dominant source of organic matter accumulating in the sinkhole changed through time: OC_T from $\sim\!3000$ to $\sim\!1500$ cal yr BP, OC_P from $\sim\!1500$ to $\sim\!1000$ cal yr BP, and OC_W from $\sim\!1000$ cal yr to present.
- From 1500 to 1000 cal yr BP, an increase in organic matter derived from primary productivity suggests an increase in nutrient residence time or concentration in the basin. The drivers of this nutrient increase appear linked to the expansion of wetlands on the adjacent epikarst surface.
- In the last 1000 years, organic matter derived from wetlands on the adjacent epikarst surface dominates deposition in Blackwood Sinkhole. Broadscale forcing from this change at ~1000 cal yr BP is unlikely sea-level change alone, given the modest changes in relative sea-level during the last 1000 years in the Bahamas. However, a decrease in local intense hurricane activity after 1000 cal yr BP, combined with changing regional precipitation may have collectively promoted wetland expansion in the last millennium.
- There are fluctuations of OC_p (20–40%) supplied to the sinkhole benthos throughout the last millennium. Further evaluation of nutrient residence time and delivery in karst basins is warranted to understand the possible linkage between primary productivity in the meteoric lens of karst basins and regional rainfall.

Acknowledgments

Additional field support was provided by Tyler Winkler, Richard Sullivan, Shawna Little, and Brian Kakuk, with technical support provided by Allison Myers-Pigg, K. Nikki West, Ren Zhang, Chris Maupin, and Amanda Fay. This research was funded by the following NSF grants: OCE-1356509 (PvH), EAR-1703087 (PvH), OCE-1356708 (JPD), BCS-1118340 (PLF), and a Student Research Grant from the Geologic Society of America (to AET, EAR-1354519). This work was improved by comments from D. Brankovits, E. Riggs, D. Thomas, and S. Feakins.

Appendix A. Supplementary data

Supplementary data associated with this article can be found in the online version at doi:https://doi.org/10.1016/j.palaeo.2018.06.014. These data include the Google map of the most important areas

described in this article.

References

- Alverez Zarikian, C.A., Swart, P.K., Gifford, J.A., Blackwelder, P.L., 2005. Holocene paleohydrology of Little Salt Spring, Florida, based on ostracod assemblages and stable isotopes. Palaeogeogr. Palaeoclimatol. Palaeoecol. 225, 134–156.
- Ashmore, S., Leatherman, S.P., 1984. Holocene sedimentation in Port Royal Bay, Bermuda. Mar. Geol. 56, 289–298.
- Blaauw, M., Christen, A., 2011. Flexible paleoclimate age-depth models using an autoregressive gamma process. Bayesian Anal. 6, 457–474.
- Brandenberger, J.M., Louchouarn, P., Crecelius, E.A., 2011. Natural and post-urbanization signatures of hypoxia in two basins of Puget Sound: historical reconstruction of redox sensitive metals and organic matter inputs. Aquat. Geochem. 17, 645–670.
- Brown, K.E., Cohen, A.D., 1995. Stratigraphic and micropetrographic occurrences of pyrite in sediments at the confluence of carbonate and peat-forming depositional systems, southern Florida, USA. Org. Geochem. 22, 105–126.
- Carew, J.L., Mylroie, J.E., 1997. Geology of the Bahamas. In: Vacher, L., Quinn, T. (Eds.), Geology and Hydrogeology of Carbonate Islands, Developments in Sedimentology. Elsevier Science Publishers, Amsterdam, pp. 91–139.
- Collins, S.V., Reinhardt, E.G., Rissolo, D., Chatters, J.C., Nava Blank, A., Luna Erreguerena, P., 2015a. Reconstructing water level in Hoyo Negro, Quintana Roo, Mexico, implications for early Paleoamerican and faunal access. Quat. Sci. Rev. 438, 124–134.
- Collins, S.V., Reinhardt, E.G., Werner, C.L., Le Maillot, C., Devos, F., Rissolo, D., 2015b. Late Holocene mangrove development and onset of sedimentation in the Yax Chen cave system (Ox Bel Ha) Yucatan Mexico: implications for using cave sediments as a sea-level indicator. Palaeogeogr. Palaeoclimatol. Palaeoecol. 438, 124–134.
- Dean Jr., W.E., 1974. Determination of carbonate and organic matter in calcareous sediments and sedimentary rocks by loss on ignition: comparison with other methods. J. Sediment. Res. 44.
- Denomee, K.C., Bentley, S.J., Droxler, A.W., 2014. Climatic control on hurricane patterns: a 1200-y near-annual record from Lighthouse Reef, Belize. Sci. Rep. 4, 7.
- Dittmar, T., Lara, R.J., Kattner, G., 2001. River or mangrove? Tracing major organic matter sources in tropical Brazilian coastal waters. Mar. Chem. 73, 253–271.
- Donnelly, J.P., Woodruff, J.D., 2007. Intense hurricane activity over the past 5,000 years controlled by El Niño and the West African monsoon. Nature 447, 465.
- Dutton, A., Bard, E., Antonioli, F., Esat, T.M., Lambeck, K., McCulloch, M.T., 2009. Phasing and amplitude of sea-level and climate change during the penultimate interglacial. Nat. Geosci. 2, 355.
- Fensterer, C., Scholz, D., Hoffmann, D., Spotl, C., Pajon, J.M., Mangini, A., 2012. Cuban stalagmite suggests relationship between Caribbean precipitation and the Atlantic Multidecadal Oscillation during the past 1.3 ka. The Holocene 22, 1405–1412.
- Fensterer, C., Scholz, D., Hoffmann, D.L., Spötl, C., Schröder-Ritzrau, A., Horn, C., Pajón, J.M., Mangini, A., 2013. Millennial-scale climate variability during the last 12.5 ka recorded in a Caribbean speleothem. Earth Planet. Sci. Lett. 361, 143–151.
- France, R.L., 1995. Carbon-13 enrichment in benthic compared to planktonic algae: foodweb implications. Mar. Ecol. Prog. Ser. 124, 307–312.
- Fritz, S.C., Björck, S., Rigsby, C.A., Baker, P.A., Calder-Church, A., Conley, D.J., 2011. Caribbean hydrological variability during the Holocene as reconstructed from crater lakes on the island of Grenada. J. Quat. Sci. 26, 829–838.
- Gamble, D.W., Parnell, D.B., Curtis, S., 2008. Spatial variability of the Caribbean midsummer drought and relation to north Atlantic high circulation. Int. J. Climatol. 28, 343–350.
- Gonneea, M.E., Paytan, A., Herrera-Silveira, J.A., 2004. Tracing organic matter sources and carbon burial in mangrove sediments over the past 160 years. Estuar. Coast. Shelf Sci. 61, 211–227.
- Gregory, B.R.B., Peros, M., Reinhardt, E.G., Donnelly, J.P., 2015. Middle–late Holocene Caribbean aridity inferred from foraminifera and elemental data in sediment cores from two Cuban lagoons. Palaeogeogr. Palaeoclimatol. Palaeoecol. 426, 229–241.
- Gregory, B.R.B., Reinhardt, E.G., Gifford, J.A., 2016. The influence of morphology on sinkhole sedimentation at Little Salt Spring, Florida. J. Coast. Res. 33, 359–371.
- Grimm, E.C., Jacobson, G.L., Watts, W.A., Hansen, B.C.S., Maasch, K.A., 1993. A 50,000-year record of climate oscillations from Florida and its temporal correlation with the Heinrich events. Science 261, 198–200.
- Grimm, E.C., Watts, W.A., Jacobson, G.L., Hansen, B.C.S., Almquist, H.R., Dieffenbacher-Krall, A.C., 2006. Evidence for warm wet Heinrich events in Florida. Quat. Sci. Rev. 25, 2197–2211.
- Hearty, P.J., Olson, S.L., Kaufman, D.S., Edwards, R.L., Cheng, H., 2004. Stratigraphy and geochronology of pitfall accumulations in caves and fissures, Bermuda. Quat. Sci. Rev. 23, 1151–1171.
- Heiri, O., Lotter, A.F., Lemcke, G., 2001. Loss on ignition as a method for estimating organic and carbonate content in sediments: reproducibility and comparability of results. J. Paleolimnol. 25, 101–110.
- van Hengstum, P.J., Reinhardt, E.G., Beddows, P.A., Gabriel, J.J., 2010. Investigating linkages between Holocene paleoclimate and paleohydrogeology preserved in a Yucatan underwater cave. Quat. Sci. Rev. 29, 2788–2798.
- van Hengstum, P.J., Scott, D.B., Gröcke, D.R., Charette, M.A., 2011. Sea level controls sedimentation and environments in coastal caves and sinkholes. Mar. Geol. 286, 35–50.
- van Hengstum, P.J., Donnelly, J.P., Toomey, M.R., Albury, N.A., Lane, P., Kakuk, B., 2014. Heightened hurricane activity on the Little Bahama Bank from 1350 to 1650 AD. Cont. Shelf Res. 86, 103–115.
- van Hengstum, P.J., Donnelly, J.P., Fall, P.L., Toomey, M.R., Albury, N.A., Kakuk, B., 2016. The intertropical convergence zone modulates intense hurricane strikes on the

- western North Atlantic margin, Sci. Rep. 6.
- van Hengstum, P.J., Maale, G., Donnelly, J.P., Albury, N.A., Onac, B.P., Sullivan, R.M., Winkler, T.S., Tamalavage, A.E., MacDonald, D., 2018. Drought in the northern Bahamas from 3300 to 2500 years ago. Quat. Sci. Rev. 186, 169–185.
- Hodell, D.A., Brenner, M., Curtis, J.H., Guilderson, T., 2001. Solar forcing of drought frequency in the Maya Lowlands. Science 292, 1367–1370.
- Hodell, D.A., Brenner, M., Curtis, J.H., 2005. Terminal Classic drought in the northern Maya lowlands inferred from multiple sediment cores in Lake Chichancanab (Mexico). Quat. Sci. Rev. 24, 1413–1427.
- Jury, M., Malmgren, B.A., Winter, A., 2007. Subregional precipitation climate of the Caribbean and relationships with ENSO and NAO. J. Geophys. Res. 112, 1–10.
- Keeley, J.E., Sandquist, D.R., 1992. Carbon: freshwater plants. Plant Cell Environ. 15, 1021–1035
- Khan, N.S., Vane, C.H., Horton, B., 2015. Stable Carbon Isotope and C/N Geochemistry of Coastal Wetland Sediments as a Sea-level Indicator. John Wiley & Sons, Ltd.
- Kjellmark, E., 1996. Late Holocene climate change and human disturbance on Andros Island, Bahamas. J. Paleolimnol. 15, 133–145.
- Kovacs, S.E., Reinhardt, E.G., Chatters, J.C., Rissolo, D., Schwarcz, H.P., Collins, S.V., Kim, S.-T., Nava Blank, A., Luna Erreguerena, P., 2017. SCalcite raft geochemistry as a hydrological proxy for Holocene aquifer conditions in Hoyo Negro and Ich Balam (Sac Actun Cave System), Quintana Roo, Mexico. Quat. Sci. Rev. 175, 97–111.
- Lamb, A.L., Wilson, G.P., Leng, M.J., 2006. A review of coastal palaeoclimate and relative sea-level reconstructions using $\delta 13C$ and C/N ratios in organic material. Earth Sci. Rev. 75, 29–57.
- Lane, P., Donnelly, J.P., Woodruff, J.D., Hawkes, A.D., 2011. A decadally-resolved paleohurricane record archived in the late Holocene sediments of a Florida sinkhole. Mar. Geol. 287, 14–30.
- Larsen, T., Wooller, M.J., Fogel, M.L., O'Brien, D.M., 2012. Can amino acid carbon isotope ratios distinguish primary producers in a mangrove ecosystem? Rapid Commun. Mass Spectrom. 26, 1541–1548.
- Loftis, K.M., Meile, C., 2014. Isotopes and elemental ratios in multi-parameter mixing models. Limnol. Oceanogr. Methods 12, 694–702.
- Mackinnon, L., Jones, B., 2001. Sedimentological evolution of North Sound, Grand Cayman-a freshwater to marine carbonate succession driven by Holocene sea-level rise. J. Sediment. Res. 71, 568–580.
- Magaña, V., Amador, J.A., Medina, S., 1999. The midsummer drought over Mexico and Central America. J. Clim. 12. 1577–1588.
- Maloof, A.C., Grotzinger, J.P., 2012. The Holocene shallowing-upward parasequence of north-west Andrso Island, Bahamas. Sedimentology 59, 1375–1407.
- Meyers, P.A., 1994. Preservation of elemental and isotopic source identification of sedimentary organic matter. Chem. Geol. 114, 289–302.
- Mylroie, J.E., Carew, J.L., Moore, A.I., 1995. Blue holes: definitions and genesis. Carbonates Evaporites 10, 225–233.
- Ogrinc, N., Fontolan, G., Faganeli, J., Covelli, S., 2005. Carbon and nitrogen isotope compositions of organic matter in coastal marine sediments (the Gulf of Trieste, N Adriatic Sea): indicators of sources and preservation. Mar. Chem. 95, 163–181.
- O'Leary, M.H., 1988. Carbon isotopes in photosynthesis. Bioscience 38, 328–336.
- Phillips, D.L., Koch, P.L., 2002. Incorporating concentration dependence in stable isotope mixing models. Oecologia 130, 114–125.
- Rasmussen, K.A., Haddad, R.I., Neuman, A.C., 1990. Stable-isotope record of organic carbon from an evolving carbonate banktop, Bight of Abaco, Bahamas. Geology 18, 790–794.
- Reimer, P.J., Bard, E., Bayliss, A., Beck, J.W., Blackwell, P.G., Bronk Ramsey, C., Buck, C.E., Cheng, H., Edwards, R.L., Friedrich, M., Grootes, P.M., Guilderson, T.P., Haflidason, H., Hajdas, I., Hatte, C., Heaton, T.J., Hoffman, D.L., Hogg, A.G., Hughen, K.A., Kaiser, K.F., Kromer, B., Manning, S.W., Niu, M., Reimer, R.W., Richards, D.A., Scott, E.M., Southon, J.R., Stafford, R.A., Turney, C.S.M., van der Plicht, J., 2013. IntCal13 and Marine13 radiocarbon age calibration curves 0–50,000 years Cal BP. Radiocarbon 55, 1869–1887.
- Richards, D.A., Smart, P.L., Edwards, R.L., 1994. Maximum sea levels for the last glacial period from U-series ages of submerged speleothems. Nature 367, 357–360.
- Richey, J.N., Sachs, J.P., 2016. Precipitation changes in the western tropical Pacific over the past millennium. Geology 44, 671–674.
- Schnurrenberger, D., Russell, J., Kelts, K., 2003. Classification of lacustrine sediments based on sedimentary components. J. Paleolimnol. 29, 141–154.
- Shinn, E.A., Reich, C.D., Locker, S.D., Hine, A.C., 1996. A giant sediment trap in the Florida Keys. J. Coast. Res. 12, 953–959.
- Slayton, I.A., 2010. A Vegetation History From Emerald Pond, Great Abaco Island, the Bahamas, Based on Pollen Analysis, Geography. University of Tennessee-Knoxville, pp. 96 (University of Tennessee-Knoxville).
- Smart, P.L., Beddows, P.A., Doerr, S., Smith, S.L., Whitaker, F.F., 2006. Cave development on the Caribbean coast of the Yucatan Peninsula, Quintana Roo, Mexico. In: Harmon, R.S., Wicks, C. (Eds.), Perspectives on Karst Geomorphology, Hydrology, and Geochemistry-a Tribute Volume to Derek C. Ford and William B. White, pp. 105–128.
- Steadman, D.W., Franz, R., Morgan, G.S., Albury, N.A., Kakuk, B., Broad, K., Franz, S.E., Tinker, K., Pateman, M.P., Lott, T.A., Jarzen, D.M., Dilcher, D.L., 2007. Exceptionally well preserved late Quaternary plant and vertebrate fossils from a blue hole on Abaco, The Bahamas. Proc. Natl. Acad. Sci. 104, 19897.
- Steadman, D.W., Albury, N.A., Maillis, P., Mead, J.I., Slapcinsky, J., Krysko, K.L., Singleton, H.M., Franklin, J., 2014. Late-Holocene faunal and landscape change in the Bahamas. The Holocene 24, 220–230.
- Talbot, M.R., Laerdal, T., 2000. The late Pleistocene-Holocene palaeolimnology of Lake Victoria, East Africa, based upon elemental and isotopic analyses of sedimentary organic matter. J. Paleolimnol. 23, 141–164.
- Taylor, K.G., Macquaker, J.H.S., 2000. Early diagenetic pyrite morphology in a mudstone-dominated succession: the Lower Jurassic Cleveland Ironstone Formation, eastern

- England. Sediment. Geol. 131, 77-86.
- Teeter, J.W., 1989. Holocene salinity history of the saline lakes of San Salvador Island, Bahamas. In: Curran, H.A., Bain, R.J., Carew, J.L., Mylroie, J., Teeter, J.W., White, B. (Eds.), Pleistocene and Holocene Carbonate Evironments on San Salvador Island, Bahamas, San Salvador, The Bahamas, pp. 35–39.
- Thornton, S.F., McManus, J., 1994. Application of organic carbon and nitrogen stable isotope and C/N ratios as source indicators of organic matter provenance in estuarine systems: evidence from the Tay Estuary, Scotland. Estuar. Coast. Shelf Sci. 38, 219–233.
- Walker, L.N., Mylorie, J.E., Walker, A.D., Mylroie, J.R., 2008. The caves of Abaco Island,
- Bahamas: keys to geologic timescales. J. Cave Karst Stud. 70, 108–119. Whitaker, F.F., Smart, P.L., 1997. Hydrogeology of Bahamian archipelago. In: Vacher, H.L., Quinn, T.M. (Eds.), Geology and Hydrogeology of Carbonate Islands:
- Developments in Sedimentology. 54. Elsevier Science Publishers, pp. 183–216. Woodruff, J.D., Donnelly, J.P., Mohrig, D., Geyer, W.R., 2008. Reconstructing relative flooding intensities responsible for hurricane-induced deposits from Laguna Playa Grande, Vieques, Puerto Rico. Geology 36, 391–394.
- Yang, C., Wilkinson, G.M., Cole, J.J., Macko, S.A., Pace, M.L., 2014. Assigning hydrogen, carbon, and nitrogen isotope values for phytoplankton and terrestrial detritus in aquatic food web studies. Inland Waters 4, 232–242.